

Supplement of Atmos. Chem. Phys., 18, 7423–7438, 2018  
<https://doi.org/10.5194/acp-18-7423-2018-supplement>  
© Author(s) 2018. This work is distributed under  
the Creative Commons Attribution 4.0 License.



*Supplement of*

## **Fine-particle pH for Beijing winter haze as inferred from different thermodynamic equilibrium models**

**Shaojie Song et al.**

*Correspondence to:* Shaojie Song (songs@seas.harvard.edu), Michael B. McElroy (mbm@seas.harvard.edu)  
and Yele Sun (sunyele@mail.iap.ac.cn)

The copyright of individual parts of the supplement might differ from the CC BY 4.0 License.

# Supplement

## Contents:

**Section S1. Revised ISORROPIA-II Model and Influence on pH Prediction**

**Section S2. Uncertainties of the AMS Measurements**

**Section S3. S-curves for gas-particle partitioning of NH<sub>3</sub>, HNO<sub>3</sub>, and HCl**

**Figures S1–S13**

**Tables S1–S8**

## Section S1. Revised ISORROPIA-II Model and Influence on pH Prediction

The revised ISORROPIA-II model in this study has fixed some coding errors in the standard ISORROPIA-II model (<http://isorro피아.eas.gatech.edu/>, last accessed: 2017/12/17). These errors are found to be closely related to aerosol water pH calculations under North China winter haze conditions. Note that only the forward stable state pH predictions are affected. Details are given in this section. The standard ISORROPIA-II model source code is password protected, but there is a version of ISORROPIA-II source code, implemented by Pye et al. (2009) into the GEOS-Chem chemical transport model and publicly accessible at <http://acmg.seas.harvard.edu/geos/doc/man/>. The code revision is available at [http://wiki.seas.harvard.edu/geos-chem/index.php/ISORROPIA\\_II#Bug\\_fixes\\_for\\_ISORROPIA\\_II\\_stable\\_mode](http://wiki.seas.harvard.edu/geos-chem/index.php/ISORROPIA_II#Bug_fixes_for_ISORROPIA_II_stable_mode) (last accessed: 2018/04/02).

### S1.1 General Solution Procedure of ISORROPIA-II

As shown in the reference manual ([http://nenes.eas.gatech.edu/ISORROPIA/Version2\\_1/ISORROPIA21Manual.pdf](http://nenes.eas.gatech.edu/ISORROPIA/Version2_1/ISORROPIA21Manual.pdf), last accessed: 2017/12/17), the ISORROPIA-II model consists of eight submodels according to the type of problem defined (forward or reverse) and the input chemical species (Table S1). For example, the submodel ISRP3F solves the forward problem for the  $\text{NH}_3\text{-Na-H}_2\text{SO}_4\text{-HNO}_3\text{-HCl-H}_2\text{O}$  aerosol system. Under each submodel, there are several subregimes determined by the molar ratios of basic chemical species ( $\text{NH}_3$ , Na, K, Ca, and Mg) to sulfuric acid (Table S2). These molar ratios are referred as “sulfate ratios”. Table S3 presents the subregimes under the submodels ISRP3F and ISRP4F. Different major and minor species potentially present in the solution are assumed by different subregimes, which reduces the number of thermodynamic reactions required. For example, gas phase  $\text{NH}_3$  is considered as a minor species for “sulfate rich” and “sulfate super-rich” aerosols, whereas bisulfate ion  $\text{HSO}_4^-$  is a minor species for “sulfate poor” aerosols.

**Table S1.** Eight submodels in ISORROPIA-II

Input Chemical Species	Submodel
$\text{NH}_3, \text{H}_2\text{SO}_4$	ISRP1F (forward) or ISRP1R (reverse)
$\text{NH}_3, \text{H}_2\text{SO}_4, \text{HNO}_3$	ISRP2F (forward) or ISRP2R (reverse)
$\text{NH}_3, \text{H}_2\text{SO}_4, \text{HNO}_3, \text{Na}, \text{HCl}$	ISRP3F (forward) or ISRP3R (reverse)
$\text{NH}_3, \text{H}_2\text{SO}_4, \text{HNO}_3, \text{Na}, \text{HCl}, \text{K}, \text{Ca}, \text{Mg}$	ISRP4F (forward) or ISRP4R (reverse)

**Table S2.** Definition of different sulfate ratios

Sulfate Ratio	Equation
Total sulfate molar ratio	$R_{\text{Total}} = \frac{[\text{NH}_3^{\text{gas+aerosol}} + \text{Na}^{\text{gas+aerosol}} + \text{Ca}^{\text{gas+aerosol}} + \text{K}^{\text{gas+aerosol}} + \text{Mg}^{\text{gas+aerosol}}]}{[\text{H}_2\text{SO}_4^{\text{gas+aerosol}}]}$
Ammonia & Sodium molar ratio	$R_{\text{NH}_3+\text{Na}} = \frac{[\text{NH}_3^{\text{gas+aerosol}} + \text{Na}^{\text{gas+aerosol}}]}{[\text{H}_2\text{SO}_4^{\text{gas+aerosol}}]}$
Crustal & Sodium molar ratio	$R_{\text{Crustal}+\text{Na}} = \frac{[\text{Na}^{\text{gas+aerosol}} + \text{Ca}^{\text{gas+aerosol}} + \text{K}^{\text{gas+aerosol}} + \text{Mg}^{\text{gas+aerosol}}]}{[\text{H}_2\text{SO}_4^{\text{gas+aerosol}}]}$
Crustal molar ratio	$R_{\text{Crustal}} = \frac{[\text{Ca}^{\text{gas+aerosol}} + \text{K}^{\text{gas+aerosol}} + \text{Mg}^{\text{gas+aerosol}}]}{[\text{H}_2\text{SO}_4^{\text{gas+aerosol}}]}$
Sodium molar ratio	$R_{\text{Na}} = \frac{[\text{Na}^{\text{gas+aerosol}}]}{[\text{H}_2\text{SO}_4^{\text{gas+aerosol}}]}$

**Table S3.** Subregimes under the submodels ISRP3F and ISRP4F

Aerosol Type	Sulfate Ratio	Subregime	Subcase
<i>ISRP3F (NH<sub>3</sub>-Na-H<sub>2</sub>SO<sub>4</sub>-HNO<sub>3</sub>-HCl-H<sub>2</sub>O aerosol)</i>			
Sulfate Poor, Sodium Rich	$R_{\text{Na}} \geq 2$	H	H1-H6
Sulfate Poor, Sodium Poor	$R_{\text{NH}_3+\text{Na}} \geq 2, R_{\text{Na}} < 2$	G	G1-G5
Sulfate Rich	$1 \leq R_{\text{NH}_3+\text{Na}} < 2$	I	I1-I6
Sulfate Super-Rich	$R_{\text{NH}_3+\text{Na}} < 1$	J	J1-J3
<i>ISRP4F (K-Ca-Mg-NH<sub>3</sub>-Na-H<sub>2</sub>SO<sub>4</sub>-HNO<sub>3</sub>-HCl-H<sub>2</sub>O aerosol)</i>			
Sulfate Poor, Crustal & Sodium Rich, Crustal Rich	$R_{\text{Crustal}} > 2$	P	P1-P13
Sulfate Poor, Crustal & Sodium Rich, Crustal Poor	$R_{\text{Crustal}+\text{Na}} \geq 2, R_{\text{Crustal}} \leq 2$	M	M1-M8
Sulfate Poor, Crustal & Sodium Poor	$R_{\text{Total}} \geq 2, R_{\text{Crustal}+\text{Na}} < 2$	O	O1-O7
Sulfate Rich	$1 \leq R_{\text{Total}} < 2$	L	L1-L9
Sulfate Super-Rich	$R_{\text{Total}} < 1$	K	K1-K4

Further, each subregime includes several subcases which depend on the input relative humidity (RH). This is because the possible solid salts have different associated deliquescence relative humidities (DRH). The RH ranges and possible solid and aqueous phases are shown in Table S4 (for subcases G1-G5) and Table S5 (for subcases O1-O7). For the stable state solution, RH increases gradually from G1 to G5 and from O1 to O7, and the solid salts are dissolved one by one (depending on their DRH). When the input RH is larger than the DRH for all possible salts, an aqueous phase always exists (G5 and O7). G5 and O7 are used thus also for the metastable state solution (no precipitate is formed).

**Table S4.** Subcases G1–G5

Subcase	RH Subdomain	Notes
G1	$RH < DRNH4NO3$	Solids: $(NH_4)_2SO_4$ , $NH_4NO_3$ , $NH_4Cl$ , $Na_2SO_4$ ; Aqueous phase: Present when $RH \geq MDRH$ .
G2	$DRNH4NO3 \leq RH < DRNH4CL$	Solids: $(NH_4)_2SO_4$ , $NH_4Cl$ , $Na_2SO_4$ ; Aqueous phase: Present when there is $NH_4NO_3$ (which deliquesces) or when $RH \geq MDRH$ .
G3	$DRNH4CL \leq RH < DRNH42S4$	Solids: $(NH_4)_2SO_4$ , $Na_2SO_4$ ; Aqueous phase: Present when there is $NH_4NO_3$ or $NH_4Cl$ (which deliquesces) or when $RH \geq MDRH$ .
G4	$DRNH42S4 \leq RH < DRNA2SO4$	Solids: $Na_2SO_4$ ; Aqueous phase: Present.
G5	$RH \geq DRNA2SO4$	Solids: None; Aqueous phase: Present; <i>This subroutine is used for the metastable mode calculation.</i>

$DRNH4NO3$ ,  $DRNH4CL$ ,  $DRNH42S4$  and  $DRNA2SO4$  represent the deliquescence relative humidity (DRH) of  $NH_4NO_{3(s)}$ ,  $NH_4Cl_{(s)}$ ,  $(NH_4)_2SO_{4(s)}$ , and  $Na_2SO_{4(s)}$ , respectively. The MDRH (mutual deliquescence relative humidity) for each subdomain represents the deliquescence point of the corresponding salt mixture and thus varies from case to case.

**Table S5.** Subcases O1–O7

Subcase	RH Subdomain	Notes
O1	$RH < DRNH4NO3$	Solids: $CaSO_4$ , $(NH_4)_2SO_4$ , $NH_4NO_3$ , $NH_4Cl$ , $MgSO_4$ , $Na_2SO_4$ , $K_2SO_4$ ; Aqueous phase: Present when $RH \geq MDRH$ .
O2	$DRNH4NO3 \leq RH < DRNH4CL$	Solids: $CaSO_4$ , $(NH_4)_2SO_4$ , $NH_4Cl$ , $MgSO_4$ , $Na_2SO_4$ , $K_2SO_4$ ; Aqueous phase: Present when there is $NH_4NO_3$ (which deliquesces) or when $RH \geq MDRH$ .
O3	$DRNH4CL \leq RH < DRNH42S4$	Solids: $CaSO_4$ , $(NH_4)_2SO_4$ , $MgSO_4$ , $Na_2SO_4$ , $K_2SO_4$ ; Aqueous phase: Present when there is $NH_4NO_3$ or $NH_4Cl$ (which deliquesces) or when $RH \geq MDRH$ .
O4	$DRNH42S4 \leq RH < DRMGSO4$	Solids: $CaSO_4$ , $MgSO_4$ , $Na_2SO_4$ , $K_2SO_4$ ; Aqueous phase: Present.
O5	$DRMGSO4 \leq RH < DRNA2SO4$	Solids: $CaSO_4$ , $Na_2SO_4$ , $K_2SO_4$ ; Aqueous phase: Present.
O6	$DRNA2SO4 \leq RH < DRK2SO4$	Solids: $CaSO_4$ , $K_2SO_4$ ; Aqueous phase: Present.
O7	$RH \geq DRK2SO4$	Solids: $CaSO_4$ ; Aqueous phase: Present; <i>This subroutine is used for the metastable mode calculation.</i>

$DRNH4NO3$ ,  $DRNH4CL$ ,  $DRNH42S4$ ,  $DRMGSO4$ ,  $DRNA2SO4$  and  $DRK2SO4$  represent the deliquescence relative humidity (DRH) of  $NH_4NO_{3(s)}$ ,  $NH_4Cl_{(s)}$ ,  $(NH_4)_2SO_{4(s)}$ ,  $MgSO_{4(s)}$ ,  $Na_2SO_{4(s)}$ , and  $K_2SO_{4(s)}$ , respectively. The MDRH (mutual deliquescence relative humidity) for each subdomain represents the deliquescence point of the corresponding salt mixture and thus varies from case to case.  $CaSO_4$  is assumed completely insoluble (Fountoukis and Nenes, 2007).

## S1.2 Coding Errors within Several Subcases

For the subcase G2 (an  $\text{NH}_3\text{-Na-H}_2\text{SO}_4\text{-HNO}_3\text{-HCl-H}_2\text{O}$  aerosol,  $R_{\text{NH}_3+\text{Na}} \geq 2$ ,  $R_{\text{Na}} < 2$ ,  $\text{DRNH}_4\text{NO}_3 \leq \text{RH} < \text{DRNH}_4\text{Cl}$ ), an aqueous phase exists if  $\text{NH}_4\text{NO}_3$  is present (which deliquesces). The problem is solved iteratively in ISORROPIA-II. For each iteration, it calculates the levels of solids, gases ( $\text{NH}_3$ ,  $\text{HNO}_3$ ,  $\text{HCl}$ ), and aqueous ions. The major ions include  $\text{Na}^+$ ,  $\text{NH}_4^+$ ,  $\text{H}^+$ ,  $\text{SO}_4^{2-}$ ,  $\text{NO}_3^-$ , and  $\text{Cl}^-$  ( $\text{HSO}_4^-$  and  $\text{OH}^-$  are considered minor species under such conditions) (Fountoukis and Nenes, 2007). The objective function is the departure of  $\text{Cl}^-_{(l)}$ ,  $\text{NH}_4^+_{(l)}$ ,  $\text{HCl}_{(g)}$ , and  $\text{NH}_{3(g)}$  from the equilibrium reaction  $\text{NH}_{3(g)} + \text{HCl}_{(g)} \leftrightarrow \text{NH}_4^+_{(l)} + \text{Cl}^-_{(l)}$ . The aerosol water pH is calculated based on ion balance:

$$\text{IB} = [\text{Na}^+_{(l)}] + [\text{NH}_4^+_{(l)}] - [\text{Cl}^-_{(l)}] - [\text{NO}_3^-_{(l)}] - 2 \times [\text{SO}_4^{2-}_{(l)}] \quad (\text{S1})$$

Here,  $[\text{Na}^+_{(l)}]$  is assumed to be zero as the RH is lower than the DRH of  $\text{Na}_2\text{SO}_{4(s)}$  and its dissolution does not affect pH. Eq. (S1) indicates that  $[\text{NH}_4^+_{(l)}]$ ,  $[\text{Cl}^-_{(l)}]$ ,  $[\text{NO}_3^-_{(l)}]$ , and  $[\text{SO}_4^{2-}_{(l)}]$  should be known in order to calculate pH.

The solution procedure begins by assuming that a very small amount of  $\text{Cl}^-_{(l)}$  exists.  $[\text{NO}_3^-_{(l)}]$  is computed taking advantage of the equilibrium reactions  $\text{HNO}_{3(g)} \leftrightarrow \text{H}^+_{(l)} + \text{NO}_3^-_{(l)}$  and  $\text{HCl}_{(g)} \leftrightarrow \text{H}^+_{(l)} + \text{Cl}^-_{(l)}$ :

$$[\text{NO}_3^-_{(l)}] = \frac{[\text{HNO}_{3(\text{T})}]}{1 + \frac{K_2}{K_1} \times \frac{\gamma_{\text{HNO}_3}^2}{\gamma_{\text{HCl}}^2} \times \frac{[\text{HCl}_{(\text{T})}] - [\text{Cl}^-_{(l)}]}{[\text{Cl}^-_{(l)}]}} \quad (\text{S2})$$

where  $K_1$  and  $K_2$  are the equilibrium constants for  $\text{HNO}_{3(g)} \leftrightarrow \text{H}^+_{(l)} + \text{NO}_3^-_{(l)}$  and  $\text{HCl}_{(g)} \leftrightarrow \text{H}^+_{(l)} + \text{Cl}^-_{(l)}$ , respectively. The symbol  $\gamma$  represents the activity coefficient. The subscript  $(\text{T})$  defines the total input.

Then,  $[\text{NH}_4^+_{(l)}]$  is calculated, which consists of two parts,  $[\text{NH}_4^+_{(l),\text{NC}}]$  (associated with  $\text{NO}_3^-_{(l)}$  and  $\text{Cl}^-_{(l)}$ ) and  $[\text{NH}_4^+_{(l),\text{S}}]$  (associated with  $\text{SO}_4^{2-}_{(l)}$ ). Thus,  $[\text{NH}_4^+_{(l)}] = [\text{NH}_4^+_{(l),\text{NC}}] + [\text{NH}_4^+_{(l),\text{S}}] \cdot [\text{SO}_4^{2-}_{(l)}]$  and  $[\text{NH}_4^+_{(l),\text{S}}]$  are computed from the equilibrium reaction  $(\text{NH}_4)_2\text{SO}_{4(s)} \leftrightarrow 2\text{NH}_4^+_{(l)} + \text{SO}_4^{2-}_{(l)}$  solving a cubic equation. Note that  $[\text{NH}_4^+_{(l),\text{S}}] = 2 \times [\text{SO}_4^{2-}_{(l)}]$ . Accordingly, Eq. (S1) becomes:

$$\text{IB} = [\text{NH}_4^+_{(l),\text{NC}}] - [\text{Cl}^-_{(l)}] - [\text{NO}_3^-_{(l)}] \quad (\text{S3})$$

Eq. (S3) indicates that the estimation of  $[\text{NH}_4^+_{(l),\text{NC}}]$  is important for pH calculation. However, we find, in the subcase G2 of the standard ISORROPIA-II model, that  $[\text{NH}_4^+_{(l),\text{NC}}]$  is wrongly calculated by Eq. (S4):

$$[\text{NH}_4^+_{(l),\text{NC}}] = \text{MIN}([\text{Cl}^-_{(l)}] + [\text{NO}_3^-_{(l)}], C_1) \quad (\text{S4})$$

where  $C_1 = [\text{NH}_{3(\text{T})}] + [\text{Na}_{(\text{T})}] - 2 \times [\text{H}_2\text{SO}_{4(\text{T})}]$ . As the iteration begins with a very small  $[\text{Cl}^-_{(\text{l})}]$  (and thus a very small  $[\text{NO}_3^-_{(\text{l})}]$ ), Eq. (S4) is usually reduced to Eq. (S5):

$$[\text{NH}_4^+_{(\text{l}),\text{NC}}] = [\text{Cl}^-_{(\text{l})}] + [\text{NO}_3^-_{(\text{l})}] \quad (\text{S5})$$

Consequently, the ion balance IB obtained from Eq. (S3) becomes zero in the subcase G2 and the pH is very often around 7 (i.e., neutral). On the other hand, the subcases G3, G4, and G5 in the ISORROPIA-II subregime G correctly calculate  $[\text{NH}_4^+_{(\text{l}),\text{NC}}]$  based on the equilibrium reaction  $\text{NH}_{3(\text{g})} + \text{H}^+_{(\text{l})} \leftrightarrow \text{NH}_4^+_{(\text{l})}$  (with an equilibrium constant  $K_3$ ) and the ion balance equation, Eq. (S1). The following equations are derived:

$$\frac{C_3([\text{NH}_4^+_{(\text{l}),\text{NC}}] + C_2)}{(C_1 - [\text{NH}_4^+_{(\text{l}),\text{NC}}])} + [\text{NH}_4^+_{(\text{l}),\text{NC}}] - [\text{Cl}^-_{(\text{l})}] - [\text{NO}_3^-_{(\text{l})}] = 0 \quad (\text{S6})$$

$$[\text{NH}_4^+_{(\text{l}),\text{NC}}]^2 - (C_1 + C_3 + [\text{Cl}^-_{(\text{l})}] + [\text{NO}_3^-_{(\text{l})}])[\text{NH}_4^+_{(\text{l}),\text{NC}}] + C_1([\text{Cl}^-_{(\text{l})}] + [\text{NO}_3^-_{(\text{l})}]) - C_2C_3 = 0 \quad (\text{S7})$$

where  $C_2 = 2 \times [\text{H}_2\text{SO}_{4(\text{T})}] - [\text{Na}_{(\text{T})}]$ ,  $C_3 = \frac{1}{K_3RT} \times \frac{\gamma_{\text{NH}_4\text{NO}_3}^2}{\gamma_{\text{HNO}_3}^2}$ ,  $R$  is the gas constant, and  $T$  is the temperature. Eq. (S7) is a quadratic equation in which  $[\text{NH}_4^+_{(\text{l}),\text{NC}}]$  is the only unknown.

The difference in calculating  $[\text{NH}_4^+_{(\text{l}),\text{NC}}]$  between G2 (using Eq. (S5)) and G3–G5 (using Eq. (S7)) is that Eq. (S7) accounts for  $\text{NH}_3$  evaporation. Note that if  $K_3 \rightarrow \infty$  (i.e.,  $\text{NH}_3$  does not evaporate), then  $C_3 \rightarrow 0$ , and Eq. (S7) is reduced to Eq. (S8), which is essentially the same as Eq. (S4).

$$([\text{NH}_4^+_{(\text{l}),\text{NC}}] - [\text{Cl}^-_{(\text{l})}] - [\text{NO}_3^-_{(\text{l})}])([\text{NH}_4^+_{(\text{l}),\text{NC}}] - C_1) = 0 \quad (\text{S8})$$

The coding errors in the subcase G2 also affect the pH calculation for the subcase G1 ( $R_{\text{NH}_3+\text{Na}} \geq 2$ ,  $R_{\text{Na}} < 2$ ,  $\text{RH} < \text{DRNH}_4\text{NO}_3$ ). An aqueous phase is present only for G1 when the RH is larger than the mutual deliquescence relative humidity (MDRH) of the salt mixture ( $(\text{NH}_4)_2\text{SO}_4$ ,  $\text{NH}_4\text{NO}_3$ ,  $\text{NH}_4\text{Cl}$ ,  $\text{Na}_2\text{SO}_4$ ) (Table S4). In this situation, the ISORROPIA model calculates a “dry” solution of chemical composition (no aqueous phase) and a “wet” solution (assuming the deliquescence of  $\text{NH}_4\text{NO}_3$ ) using results from the subcase G2. The actual gas/liquid/solid composition is then a weighted average of the “dry” and “wet” solutions (Fountoukis and Nenes, 2007). The molar concentrations of chemical species in the aqueous phase are the same as the results from G2, and thus the aerosol water pH in G1 is the same as that in G2.

Similar coding errors are found also for the subcases O1 and O2 ( $\text{K-Ca-Mg-NH}_3\text{-Na-H}_2\text{SO}_4\text{-HNO}_3\text{-HCl-H}_2\text{O}$  aerosol,  $R_{\text{Total}} \geq 2$ ,  $R_{\text{Crustal+Na}} < 2$ ; see Tables S3 and S5). Because the standard ISORROPIA-II model fails to account for  $\text{NH}_3$  evaporation, the calculated aerosol water pH is very often  $\sim 7$  for O1 and O2.

Overall, we have identified coding errors in the standard ISORROPIA-II model which are related to the calculation of aerosol water pH for the four subcases (G1, G2, O1, and O2). It is important to note that only the forward stable mode calculations are affected by these errors. The forward metastable mode solutions remain the same since other subcases (G5 and O7) are used. It is also important to note that these errors have little effect on the predicted gas phase  $\text{NH}_3$  levels. In ISORROPIA-II, the gas phase  $\text{NH}_3$  is computed from the difference between the total  $\text{NH}_3$  and aqueous phase  $\text{NH}_4^+$ . The difference caused by these coding errors is equal to  $[\text{H}^+_{(l)}]$ , much smaller than  $[\text{NH}_4^+_{(l)}]$ . In addition, the same coding issues also exist in previous ISORROPIA versions 1.5 and 1.7.

In this study, the ISORROPIA-II model with these coding errors fixed is denoted as the revised ISORROPIA-II model, which is used to predict aerosol water and pH in the stable state.

### S1.3 Sensitivity Tests

In order to explore the effect of our model revisions on the aerosol water pH calculations in ISORROPIA-II, we have carried out two sets of sensitivity tests. The first is for an  $\text{NH}_3\text{-Na-H}_2\text{SO}_4\text{-HNO}_3\text{-HCl-H}_2\text{O}$  aerosol system (Fig. S1). The forward metastable mode and forward stable mode simulations are performed for the standard ISORROPIA-II model; for the revised ISORROPIA-II model, only the forward stable mode simulations are made. The input data of Na,  $\text{HNO}_3$ , HCl, RH, and temperature are fixed, which represent the average  $\text{PM}_{10}$  (particles with size smaller than 1  $\mu\text{m}$ ) observations of Beijing winter haze pollution episodes reported by Wang et al. (2016), and are summarized in Table S6. The levels of  $\text{H}_2\text{SO}_4$  and  $\text{NH}_3$  are varied over large ranges. As shown in Fig. S1d, three subcases (G1, I3, and J3) are included in these sensitivity tests. Our model revisions have no effect on I3 and J3. For G1, the standard forward stable mode simulations almost always predict pH around 7 (Fig. S1b), whereas the standard forward metastable mode simulations and the revised forward stable mode simulations predict similar values for  $\text{pH} < 7$  (Fig. S1a-c). It is also seen from Fig. S1 that Beijing winter haze conditions fall within the subcase G1. Thus, our model revisions have a significant impact on estimating Beijing winter haze aerosol pH.

The second set of sensitivity tests is for a  $\text{K-Ca-Mg-NH}_3\text{-Na-H}_2\text{SO}_4\text{-HNO}_3\text{-HCl-H}_2\text{O}$  aerosol. The ISORROPIA-II model simulations are analogous to those in the first set. The levels of  $\text{H}_2\text{SO}_4$  and  $\text{NH}_3$  are varied whereas the other inputs which represent the average  $\text{PM}_{2.5}$  observations of Xi'an winter haze pollution episodes reported by Wang et al. (2016) are fixed. As shown in Fig. S2, our model revisions change the pH output (from  $\sim 7$  to  $< 7$ ) in the subcase O1 (most of the Xi'an winter haze conditions fall within O1), but do not affect the other subcases (P5, M1, L3, and K3). In addition, some non-monotonic features (i.e., noises) of the pH output are observed in Figs. S1 and S2 for all of the ISORROPIA-II simulations, when the total molar concentrations of basic species ( $[\text{K}_{(T)}] + 2 \times [\text{Ca}_{(T)}] + 2 \times [\text{Mg}_{(T)}] + [\text{Na}_{(T)}] + [\text{NH}_{3(T)}]$ ) are smaller than those of acidic species ( $2 \times [\text{H}_2\text{SO}_{4(T)}] + [\text{HNO}_{3(T)}] + [\text{HCl}_{(T)}]$ ). Such noises are due likely to instability of the numerical solver used in ISORROPIA-II. This issue is currently being investigated by Dr. Sebastian D. Eastham ([wiki.seas.harvard.edu/geos-chem/index.php/ISORROPIA\\_II](http://wiki.seas.harvard.edu/geos-chem/index.php/ISORROPIA_II), last accessed: 2017/12/01). Fortunately, this issue does not strongly affect the pH calculation results under North China winter haze conditions.

**Table S6.** Summary of gases and aerosol measurements in Beijing and Xi'an reported by Wang et al. (2016)

	Beijing Polluted		Xi'an Polluted	
Year	2015		2012	
PM size	PM <sub>1</sub>		PM <sub>2.5</sub>	
	Mean	Range	Mean	Range
SO <sub>4</sub> <sup>2-</sup> , μg m <sup>-3</sup>	26	20–38	38	20–83
NO <sub>3</sub> <sup>-</sup> , μg m <sup>-3</sup>	26	4.5–48	33	12–55
Cl <sup>-</sup> , μg m <sup>-3</sup>	1.7	0.0–4.5	14	2.6–34
NH <sub>4</sub> <sup>+</sup> , μg m <sup>-3</sup>	20	9.1–30	25	3.2–44
Na <sup>+</sup> , μg m <sup>-3</sup>	NA	NA	4.2	0.5–17
K <sup>+</sup> , μg m <sup>-3</sup>	NA	NA	4.6	1.8–8.3
Ca <sup>2+</sup> , μg m <sup>-3</sup>	NA	NA	2.3	0.2–5.9
Mg <sup>2+</sup> , μg m <sup>-3</sup>	NA	NA	0.3	0.0–0.8
NH <sub>3</sub> , ppb	17	10–32	23	9.3–61
T, °C	0.9	-1.7–8.2	4.1	-3.1–14
RH, %	56	22–72	68	41–93

NA = Not Available. The polluted condition is defined by the concentration of SO<sub>4</sub><sup>2-</sup> > 20 μg m<sup>-3</sup>.

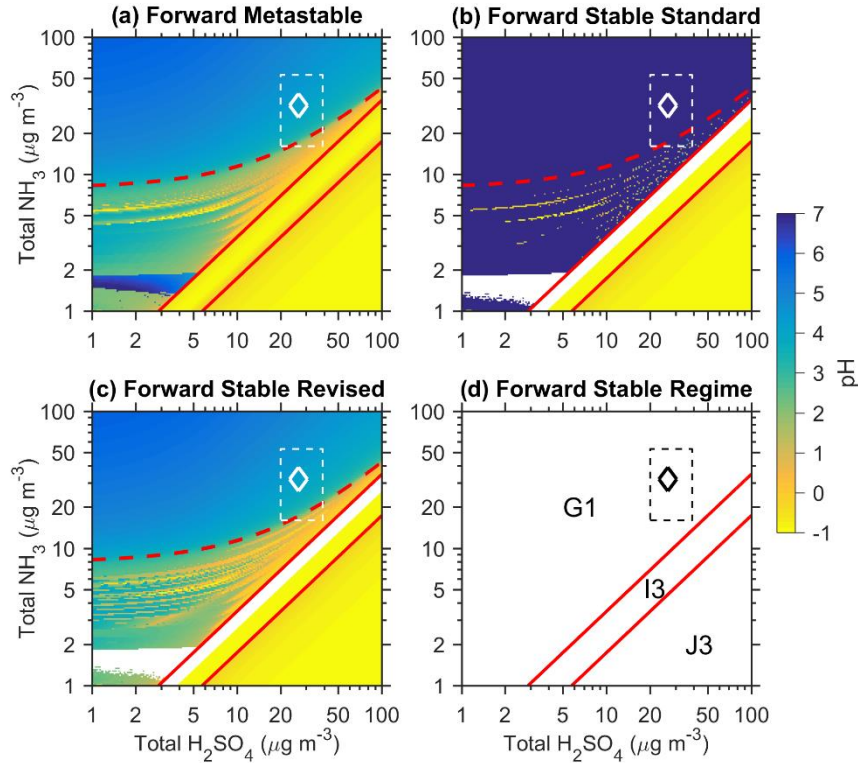


**Figure S1.** Sensitivity of pH to the total (gas + aerosol) NH<sub>3</sub> and H<sub>2</sub>SO<sub>4</sub> concentrations. The results reflect thermodynamic equilibrium predictions with different ISORROPIA-II model assumptions: (a) forward metastable mode, (b) standard forward stable mode, and (c) revised forward stable mode. The subregimes of the ISORROPIA-II forward stable mode are shown in panel (d). The solid red curves are used to distinguish different subregimes. The chemical and meteorological input data (total Na = 0 μg m<sup>-3</sup>, total HNO<sub>3</sub> = 26 μg m<sup>-3</sup>, total HCl = 1.7 μg m<sup>-3</sup>, RH = 56%, T = 274.1 K) for the NH<sub>3</sub>-Na-H<sub>2</sub>SO<sub>4</sub>-HNO<sub>3</sub>-HCl-H<sub>2</sub>O aerosol

system reflect average PM<sub>1</sub> measurements for Beijing winter haze pollution episodes reported by Wang et al. (2016). The dashed red curves indicate the situation in which the total molar concentrations of acidic and basic species are equal ( $[\text{Na}_{(\text{T})}] + [\text{NH}_{3(\text{T})}] = 2 \times [\text{H}_2\text{SO}_{4(\text{T})}] + [\text{HNO}_{3(\text{T})}] + [\text{HCl}_{(\text{T})}]$ ). Boxes define observed concentration ranges for the Beijing winter haze pollution episodes and diamonds represent the average Beijing haze conditions (total NH<sub>3</sub> = 32 μg m<sup>-3</sup>, total H<sub>2</sub>SO<sub>4</sub> = 26 μg m<sup>-3</sup>).

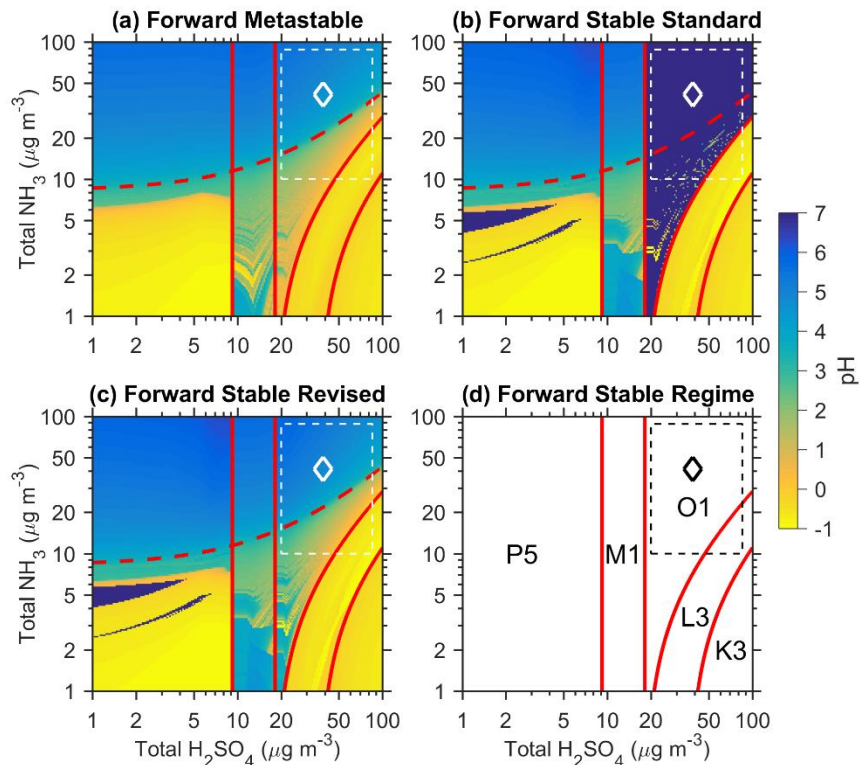


**Figure S2.** Sensitivity of pH to the total (gas + aerosol) NH<sub>3</sub> and H<sub>2</sub>SO<sub>4</sub> concentrations. The results reflect thermodynamic equilibrium predictions with different ISORROPIA-II model assumptions: (a) forward metastable mode, (b) standard forward stable mode, and (c) revised forward stable mode. The subregimes of the ISORROPIA-II forward stable mode are shown in panel (d). The solid red curves are used to distinguish different subregimes. The chemical and meteorological input data (total Na = 4.2 μg m<sup>-3</sup>, total K = 4.6 μg m<sup>-3</sup>, total Ca = 2.3 μg m<sup>-3</sup>, total Mg = 0.3 μg m<sup>-3</sup>, total HNO<sub>3</sub> = 34 μg m<sup>-3</sup>, total HCl = 14 μg m<sup>-3</sup>, RH = 68%, T = 277.3 K) for the K–Ca–Mg–NH<sub>3</sub>–Na–H<sub>2</sub>SO<sub>4</sub>–HNO<sub>3</sub>–HCl–H<sub>2</sub>O aerosol system reflect average PM<sub>2.5</sub> measurements for Xi'an winter haze pollution episodes reported by Wang et al. (2016). The dashed red curves indicate the situation in which the total molar concentrations of acidic and basic species are equal ( $[\text{K}_{(\text{T})}] + 2 \times [\text{Ca}_{(\text{T})}] + 2 \times [\text{Mg}_{(\text{T})}] + [\text{Na}_{(\text{T})}] + [\text{NH}_{3(\text{T})}] = 2 \times [\text{H}_2\text{SO}_{4(\text{T})}] + [\text{HNO}_{3(\text{T})}] + [\text{HCl}_{(\text{T})}]$ ). Boxes define observed concentration ranges for Xi'an winter haze pollution episodes and diamonds represent the average Xi'an haze conditions (total NH<sub>3</sub> = 41 μg m<sup>-3</sup>, total H<sub>2</sub>SO<sub>4</sub> = 39 μg m<sup>-3</sup>).

We also calculate particle pH using our observational data collected during 2014 winter in Beijing and the standard and revised ISORROPIA-II models (Fig. S3). As expected, predicted pH values are different for the subcases G1, G2, O1, and O2. The predicted  $\text{NH}_{3(g)}$  from the standard and revised calculations are similar and thus it is impossible to differentiate them by comparing the  $\text{NH}_{3(g)}$  concentrations. Similarly, predicted particle  $\text{NH}_4^+$  concentrations from the standard and revised model calculations should also be similar (because in the forward-mode calculations the total (gas + aerosol) quantity is fixed). Therefore, we believe that the measurement–model comparisons of  $\text{NH}_3$  gas-particle partitioning for the standard ISORROPIA-II forward stable mode calculations cannot be used to evaluate the success or failure of pH predictions, in contrast to previous studies (Wang et al., 2016; Guo et al., 2017). The subtle difference  $\Delta\text{NH}_3$  ( $< 1 \times 10^{-3}$  ppb) shown in Figs. S3c and f suggests that incorporating the partitioning of  $\text{NH}_3$  in the revised calculations pushes a little more ammonia to the gas phase, and thus more  $\text{H}^+$  is needed in the aqueous phase and the solution is more acidic.

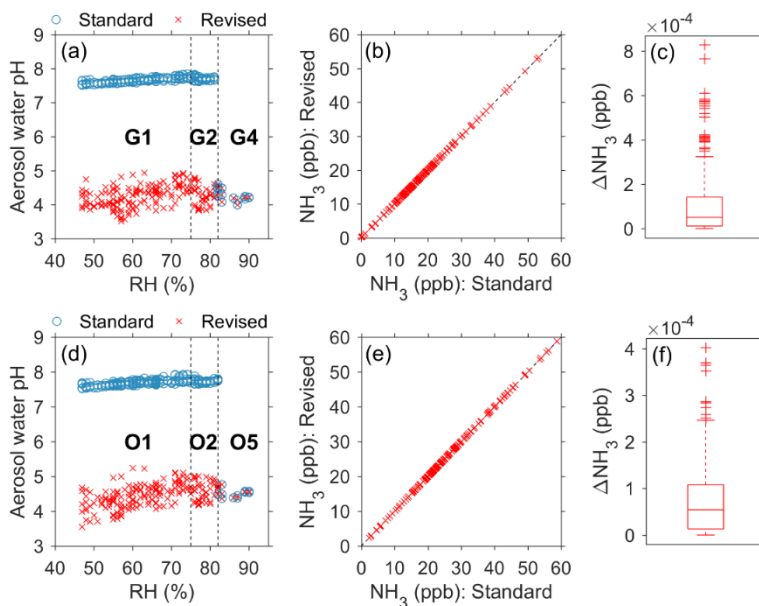


**Figure S3.** Comparisons of the predicted pH and gas phase  $\text{NH}_3$  concentrations between the standard and revised ISORROPIA-II models with the stable state assumptions. (a–c) show the results using the AMS  $\text{PM}_{10}$  measurements (an  $\text{NH}_3\text{--H}_2\text{SO}_4\text{--HNO}_3\text{--HCl--H}_2\text{O}$  aerosol), and (d–f) show the results using the GAC-IC  $\text{PM}_{2.5}$  measurements (a  $\text{K--NH}_3\text{--Na--H}_2\text{SO}_4\text{--HNO}_3\text{--HCl--H}_2\text{O}$  aerosol).

## Section S2. Uncertainties of the AMS Measurements

The AMS measurement uncertainty arises from inaccuracies in the ionization efficiency of nitrate ( $IE_{NO_3}$ ), the relative ionization efficiency of a species  $X$  relative to nitrate ( $RIE_X$ ), the collection efficiency (CE), flow rate (Q), and the transmission efficiency (TE):

$$\frac{\Delta_X}{X} = \sqrt{\left(\frac{\Delta IE_{NO_3}}{IE_{NO_3}}\right)^2 + \left(\frac{\Delta RIE_X}{RIE_X}\right)^2 + \left(\frac{\Delta CE}{CE}\right)^2 + \left(\frac{\Delta Q}{Q}\right)^2 + \left(\frac{\Delta TE}{TE}\right)^2} \quad (S9)$$

where  $\frac{\Delta IE_{NO_3}}{IE_{NO_3}}$ ,  $\frac{\Delta CE}{CE}$ ,  $\frac{\Delta Q}{Q}$ , and  $\frac{\Delta TE}{TE}$  are estimated to be 10%, 30%, <0.5%, and 10%, respectively; and  $\frac{\Delta RIE_X}{RIE_X}$  depends on the species  $X$  (10% for ammonium, 15% for sulfate and 20% for organics) (Bahreini et al., 2009). Using the above equation, we estimate that the overall relative uncertainties of the AMS measurements are 33% (nitrate), 35% (ammonium), 36% (sulfate), and 39% (organics). The relative uncertainties for chloride and black carbon have not been quantified and are assumed to be 40% in this study.

### Section S3. S-curves for gas-particle partitioning of NH<sub>3</sub>, HNO<sub>3</sub>, and HCl

Note that we assume water activity and all of the activity coefficients equal to unity (i.e., an ideal aqueous solution).

#### S3.1 NH<sub>3</sub>

The ammonia–water equilibrium is (Seinfeld and Pandis, 2016)



Their equilibrium constants can be expressed as  $H_{\text{NH}_3} = \frac{[\text{NH}_3 \cdot \text{H}_2\text{O} (l)]}{p_{\text{NH}_3}}$  and  $K_a = \frac{[\text{NH}_4^+ (l)][\text{OH}^-]}{[\text{NH}_3 \cdot \text{H}_2\text{O} (l)]} = \frac{[\text{NH}_4^+ (l)][\text{H}^+]}{K_w [\text{NH}_3 \cdot \text{H}_2\text{O} (l)]}$ , where  $H_{\text{NH}_3}$  (M atm<sup>-1</sup>) is the Henry's law constant for NH<sub>3</sub>,  $p_{\text{NH}_3}$  (atm) is the partial pressure for NH<sub>3</sub>,  $K_a$  (M) is the dissociation equilibrium constant for NH<sub>3</sub>·H<sub>2</sub>O,  $K_w$  (M<sup>2</sup>) is the dissociation equilibrium constant for water, and [X] represents aqueous concentrations of the species X (M). Thus, the total ammonia concentration in the liquid phase is

$$[\text{NH}_4^+ (T)] = [\text{NH}_3 \cdot \text{H}_2\text{O} (l)] + [\text{NH}_4^+ (l)] = H_{\text{NH}_3} p_{\text{NH}_3} \left(1 + \frac{K_a}{[\text{OH}^-]}\right) = H_{\text{NH}_3} p_{\text{NH}_3} \left(1 + \frac{K_a [\text{H}^+]}{K_w}\right) \quad (\text{S12})$$

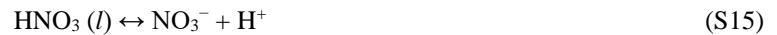
Under neutral or acidic conditions,  $\frac{K_a [\text{H}^+]}{K_w} \gg 1$ , and thus  $[\text{NH}_4^+ (T)] \cong \frac{H_{\text{NH}_3} K_a}{K_w} [\text{H}^+] p_{\text{NH}_3}$ . The aqueous fraction of total (gas + particle) ammonia,  $\varepsilon(\text{NH}_4^+)$ , is calculated as

$$\varepsilon(\text{NH}_4^+) = \frac{\frac{H_{\text{NH}_3} K_a}{K_w} [\text{H}^+] p_{\text{NH}_3} W}{\frac{H_{\text{NH}_3} K_a}{K_w} [\text{H}^+] p_{\text{NH}_3} W + \frac{p_{\text{NH}_3}}{RT}} = \frac{H_{\text{NH}_3}^* \text{WRT}}{1 + H_{\text{NH}_3}^* \text{WRT}} \quad (\text{S13})$$

where W is the aerosol water content, R is the ideal gas constant, T is the ambient temperature, and  $H_{\text{NH}_3}^* = \frac{H_{\text{NH}_3} K_a}{K_w} [\text{H}^+]$  is known as the effective Henry's law coefficient for NH<sub>3</sub>.

#### S3.2 HNO<sub>3</sub>

The nitric acid–water equilibrium is (Seinfeld and Pandis, 2016)



The equilibrium constants for these two equations are  $H_{\text{HNO}_3} = \frac{[\text{HNO}_3 (l)]}{p_{\text{HNO}_3}}$  and  $K_{nl} = \frac{[\text{NO}_3^- (l)][\text{H}^+]}{[\text{HNO}_3 (l)]}$ , where  $H_{\text{HNO}_3}$  (M atm<sup>-1</sup>) is the Henry's law constant of HNO<sub>3</sub>,  $p_{\text{HNO}_3}$  (atm) is the partial pressure of HNO<sub>3</sub>, and  $K_{nl}$  is the dissociation equilibrium constant. The total nitrate in the liquid phase can be expressed as

$$[\text{NO}_3^-] = \frac{H_{\text{HNO}_3} K_{nl}}{[\text{H}^+]} p_{\text{HNO}_3} \quad (\text{S16})$$

The aqueous fraction of total (gas + particle) nitric acid,  $\varepsilon(\text{NO}_3^-)$ , is calculated as

$$\varepsilon(\text{NO}_3^-) = \frac{\frac{H_{\text{HNO}_3} K_{nl}}{[\text{H}^+]} p_{\text{HNO}_3} W}{\frac{H_{\text{HNO}_3} K_{nl}}{[\text{H}^+]} p_{\text{HNO}_3} W + \frac{p_{\text{HNO}_3}}{RT}} = \frac{H_{\text{HNO}_3}^* WRT}{1 + H_{\text{HNO}_3}^* WRT} \quad (\text{S17})$$

where  $W$  is the aerosol water content,  $R$  is the ideal gas constant,  $T$  is the ambient temperature, and  $H_{\text{HNO}_3}^* = \frac{H_{\text{HNO}_3} K_{nl}}{[\text{H}^+]}$  is the effective Henry's law coefficient.

### S3.3 HCl

Similar to the nitric acid-water equilibrium, the hydrochloric acid-water equilibrium is (Seinfeld and Pandis, 2016)



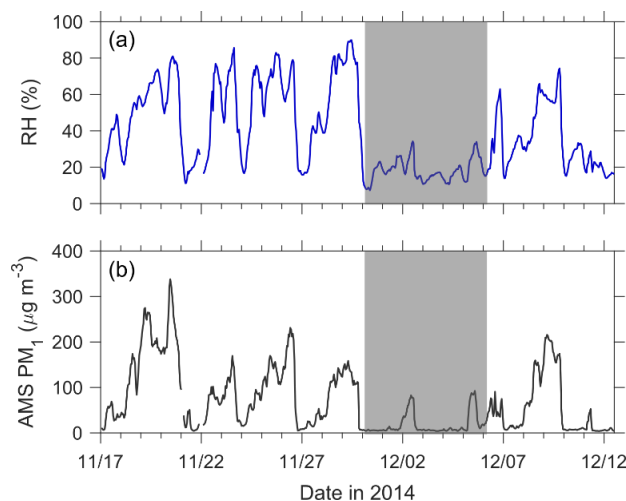
The equilibrium constants for these two equations are  $H_{\text{HCl}} = \frac{[\text{HCl}(l)]}{p_{\text{HCl}}}$  and  $K_{n2} = \frac{[\text{Cl}^-][\text{H}^+]}{[\text{HCl}(l)]}$ , where  $H_{\text{HCl}}$  ( $\text{M atm}^{-1}$ ) is the Henry's law constant of HCl,  $p_{\text{HCl}}$  (atm) is the partial pressure of HCl,  $K_{n2}$  is the dissociation equilibrium constant of  $\text{HCl}(l)$ . The total  $[\text{Cl}^-]$  in the liquid phase can be expressed as

$$[\text{Cl}^-] = \frac{H_{\text{HCl}} K_{n2}}{[\text{H}^+]} p_{\text{HCl}} \quad (\text{S20})$$

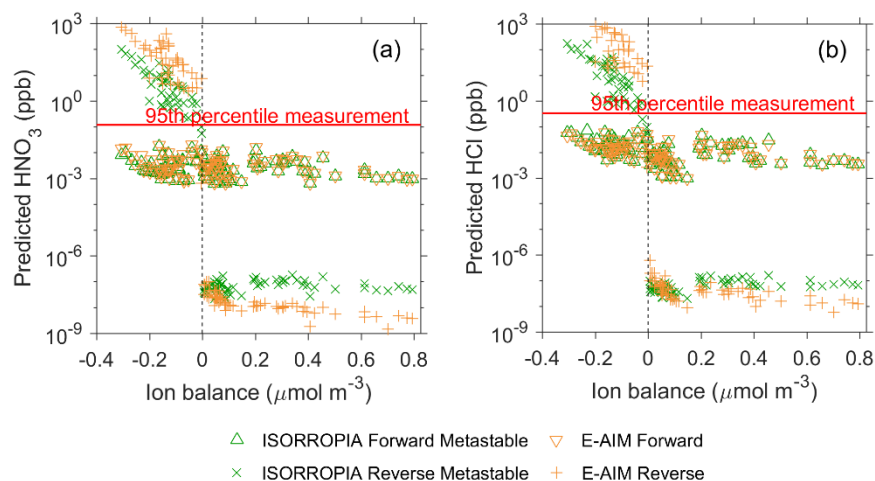
The aqueous fraction of total (gas + particle) hydrochloric acid,  $\varepsilon(\text{Cl}^-)$ , is calculated as

$$\varepsilon(\text{Cl}^-) = \frac{\frac{H_{\text{HCl}} K_{n2}}{[\text{H}^+]} p_{\text{HCl}} W}{\frac{H_{\text{HCl}} K_{n2}}{[\text{H}^+]} p_{\text{HCl}} W + \frac{p_{\text{HCl}}}{RT}} = \frac{H_{\text{HCl}}^* WRT}{1 + H_{\text{HCl}}^* WRT} \quad (\text{S21})$$

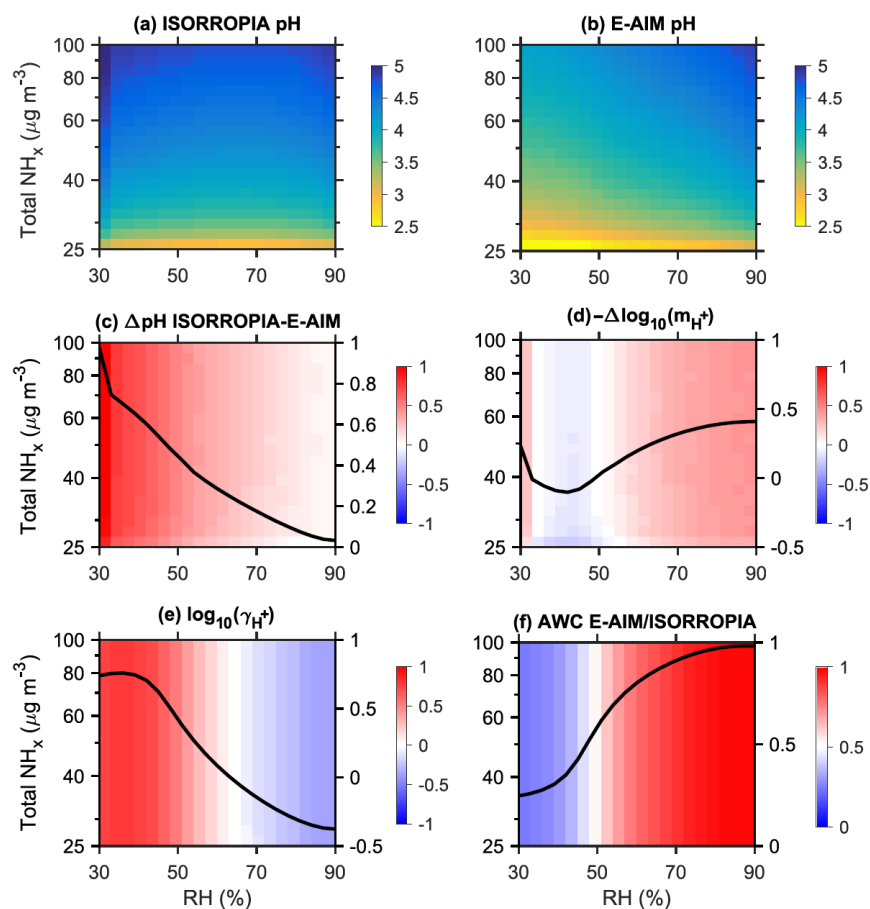
where  $W$  is the aerosol water content,  $R$  is the ideal gas constant,  $T$  is the ambient temperature, and  $H_{\text{HCl}}^* = \frac{H_{\text{HCl}} K_{n2}}{[\text{H}^+]}$  is known as the effective Henry's law coefficient for hydrochloric acid.



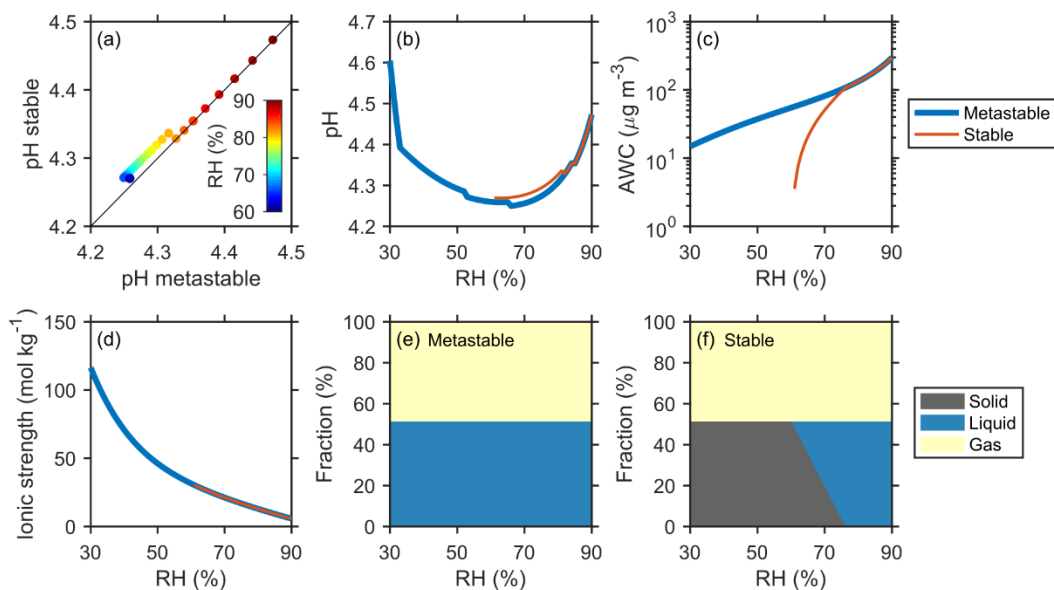
**Figure S4.** Time series of measured RH (a) and AMS PM<sub>1</sub> concentrations (b). The shaded area indicates a time period of ~ 6 days which were very dry (with RH from 7% to 34%) and relatively clean, and thus were not included in the thermodynamic analysis.



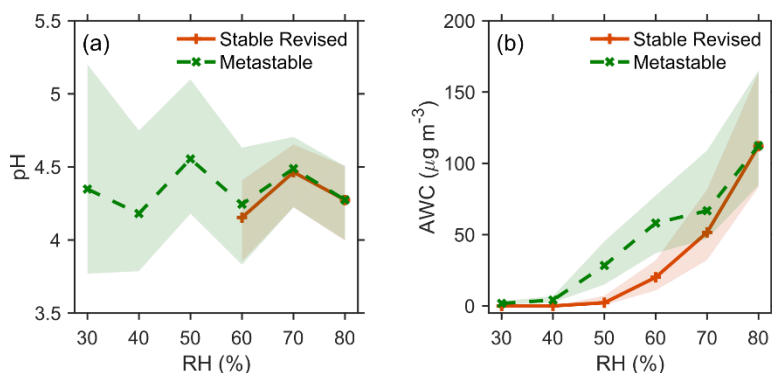
**Figure S5.** Relationship between ion balance and gas phase HNO<sub>3</sub> (a) and HCl (b) mixing ratios predicted using forward and reverse mode calculations. It is seen that the reverse mode calculations predict either very high or very low levels of HNO<sub>3</sub> and HCl depending on the sign (negative or positive) of the ion balance, whereas forward mode predictions are insensitive to ion balance. Because the measured mixing ratios of HNO<sub>3</sub> and HCl are very low and sometimes below detection limits, we do not present a quantitative comparison but show the 95% percentile of the HNO<sub>3</sub> and HCl data in our measurement period. As shown, the very high levels of HNO<sub>3</sub> and HCl in the reverse mode calculations (corresponding to negative ion balance, cations < anions, and low pH values, see Fig. 1 in the main text) are unlikely to be detected in the atmosphere.



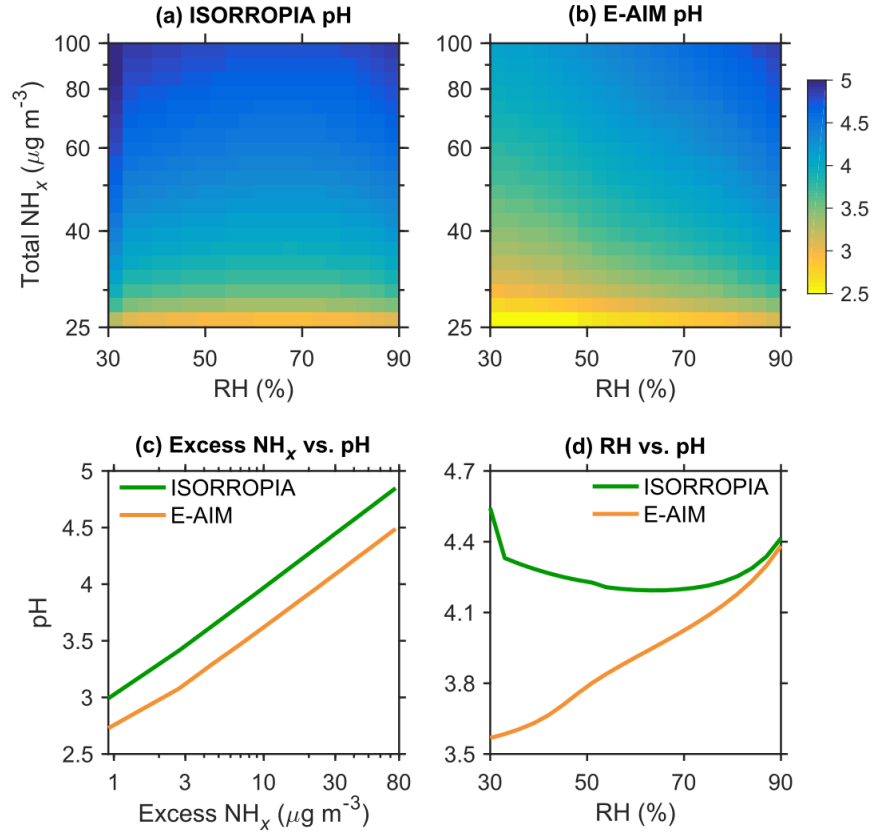
**Figure S6.** Comparison of predicted pH and several other parameters by ISORROPIA and E-AIM (version II) under representative Beijing winter haze conditions ( $\text{NH}_x$ -rich). These variables are shown as a function of RH and total  $\text{NH}_x$  concentrations. pH from ISORROPIA (a), pH from E-AIM (b),  $\Delta\text{pH}$  (ISORROPIA - E-AIM) (c),  $-\Delta\log_{10} m_{\text{H}^+}$  (d),  $\log_{10} \gamma_{\text{H}^+}$  (e), and the ratio of AWC between E-AIM and ISORROPIA (f). The curve in each panel (c–f) shows the average value for each bin of RH. E-AIM (version II) and ISORROPIA are run in the forward metastable mode. The model inputs are calculated as the average values during haze episodes ( $\text{RH} > 60\%$ ) from our field measurements in Beijing, which include total (gas + particle)  $\text{H}_2\text{SO}_4 = 30 \mu\text{g m}^{-3}$ , total  $\text{HNO}_3 = 51 \mu\text{g m}^{-3}$ , and temperature = 278 K. The total  $\text{NH}_x$  concentrations and RH vary from 25 to 100  $\mu\text{g m}^{-3}$  and from 30% to 90%, respectively.  $\text{Na}^+$  and  $\text{K}^+$  are accounted for as equivalent  $\text{NH}_4^+$ , and  $\text{Cl}^-$  as equivalent  $\text{NO}_3^-$ . The average total  $\text{NH}_x$  concentration in our measurements is 47  $\mu\text{g m}^{-3}$ . Note that the y axis is in log scale.



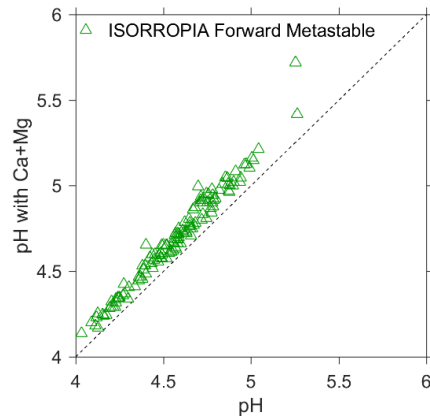
**Figure S7.** Comparisons of the ISORROPIA predicted pH (a–b), AWC (c), ionic strength (d), and partitioning of  $\text{NH}_3$  (e–f) under assumptions of the metastable and stable phase states. The model inputs include total  $\text{H}_2\text{SO}_4 = 30 \mu\text{g m}^{-3}$ , total  $\text{HNO}_3 = 51 \mu\text{g m}^{-3}$ , total  $\text{NH}_x = 47 \mu\text{g m}^{-3}$ , temperature = 278 K, and varied RH values. The inputs are calculated from our field measurements during haze episodes ( $\text{RH} > 60\%$ ) as the average temperature and the average concentrations of total  $\text{H}_2\text{SO}_4$ ,  $\text{HNO}_3$ , and  $\text{NH}_x$ .  $\text{Na}^+$  and  $\text{K}^+$  are accounted for as equivalent  $\text{NH}_4^+$ , and  $\text{Cl}^-$  as equivalent  $\text{NO}_3^-$ . When the RH is between about 60% and about 80% (when both aqueous and solid phases are present for the stable solution), the predicted pH values for the stable solution are on average  $0.02 \pm 0.00$  greater than those for the metastable solution. This difference in pH is small relative to the uncertainty resulting from other factors (e.g., measurements of gas and aerosol species and meteorological parameters).



**Figure S8.** pH (a) and AWC (b) predicted by the AMS  $\text{PM}_{10}$  measurements and forward-mode ISORROPIA calculations using both stable and metastable state assumptions. Data are grouped in RH bins (10% increment). The shaded regions indicate the 25<sup>th</sup> and 75<sup>th</sup> percentiles. Note that the revised ISORROPIA model is used for the stable state. The uncertainties of ionic and gas measurements are considered using a Monte Carlo approach.



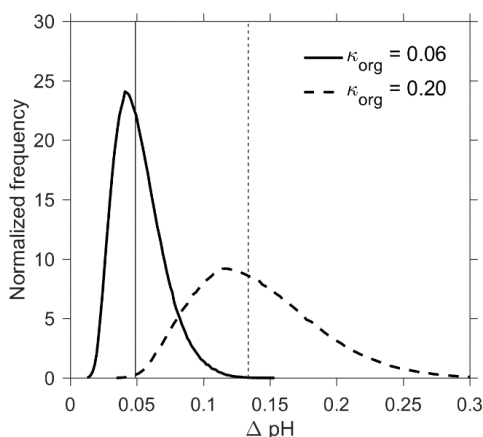
**Figure S9.** Sensitivity of particle pH to excess  $\text{NH}_x$  and RH. The model simulations conducted are the same as in Fig. S6. The required  $\text{NH}_x$  concentrations calculated for the input total  $\text{H}_2\text{SO}_4$  and  $\text{HNO}_3$  concentrations are  $24 \mu\text{g m}^{-3}$ . The curves in panels (c) and (d) show the average pH in each bin of  $\text{NH}_x$  concentrations or RH. Note that the y axis in panel (a–b) and the x axis in panel (c) are in log scale.



**Figure S10.** Sensitivity of Ca and Mg on particle pH evaluated using ISORROPIA forward metastable calculations. Based on the measured mass concentrations of  $\text{Na}^+$ ,  $\text{K}^+$ ,  $\text{Ca}^{2+}$ , and  $\text{Mg}^{2+}$  in previous studies (summarized in Table S7), the concentration of  $\text{Ca}^{2+}$  is rarely higher than  $\text{K}^+$ , and  $\text{Mg}^{2+}$  is rarely higher than 20% of  $\text{K}^+$  concentration. Thus we make a sensitivity test by assuming that  $\text{Ca}^{2+}$  equals to  $\text{K}^+$  and that the concentration of  $\text{Mg}^{2+}$  is 20% of  $\text{K}^+$ . Results show, during winter haze events ( $\text{RH} > 60\%$ ), that including  $\text{Ca}^{2+}$  and  $\text{Mg}^{2+}$  in the calculations increases the predicted particle pH by  $0.12 \pm 0.05$  unit.

**Table S7.** Mass concentrations of crustal species in PM<sub>2.5</sub> measured in Beijing during winter haze events ( $\mu\text{g m}^{-3}$ )

Studies/Species	Na <sup>+</sup>	K <sup>+</sup>	Ca <sup>2+</sup>	Mg <sup>2+</sup>
Jiang et al. (2016)	2.0±0.9	2.9±0.4	2.9±1.8	0.4±0.2
Yang et al. (2015)	0.9±0.3	1.4±0.9	0.5±0.3	0.1±0.1
Huang et al. (2014)	1.0±0.5	4.2± 2.1	0.4± 0.3	0.2±0
Liu et al. (2017) case 1	0.9±0.2	1.8±0.5	0.8±0.2	0.1±0.0
Liu et al. (2017) case 2	0.5±0.1	0.4±0.2	0.1±0.1	0.1±0.0
Liu et al. (2017) case 3	0.8±0.2	0.6±0.3	0.04	0.04

**Figure S11.** The potential impact of aerosol water associated with organic compounds and black carbon on the predicted fine particle pH. The pH values are obtained from the ISORROPIA forward mode metastable calculations. The uncertainties of ionic and gas measurements are considered using a Monte Carlo approach. The solid and dashed curves use  $\kappa_{\text{org}}$  of 0.06 and 0.20, respectively, and both use a  $\kappa$  of 0.04 for black carbon. The vertical lines indicate the average  $\Delta\text{pH}$  values of 0.05 and 0.13, respectively.**Table S8.** Mass concentrations of major organic acid salts in PM<sub>2.5</sub> measured in urban Beijing during winter ( $\text{ng m}^{-3}$ )

Reference	Wang et al. (2007)	Huang et al. (2005)	Du et al. (2014)	Jiang et al. (2016)	Wang et al. (2017)
Year	2002	2003	2010	2014	2014
Oxalic	477±304	107±35	195±137	441±429	166±157
Malonic		28±12			16±11
Succinic		24±7			36±26
Glutaric		10±4			5±4
Formic	178±81				
Acetic	3±3				
Glyoxylic		18±5			20±23
Pyruvic		31±14			15±9

Blank means not measured.

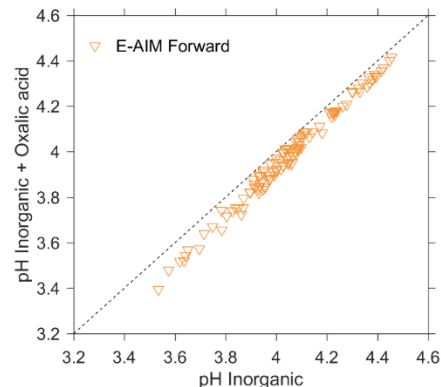


**Figure S12.** The potential impact of oxalic acid on particle pH evaluated using the E-AIM forward-mode calculations. The  $x$  axis defines the pH values when only inorganic species ( $\text{Na}^+$ ,  $\text{NH}_4^+$ ,  $\text{SO}_4^{2-}$ ,  $\text{NO}_3^-$ , and  $\text{Cl}^-$ ) are included in the aerosol system, and the  $y$  axis indicates the pH values when oxalate is also included. The dashed line indicates a 1:1 relationship.

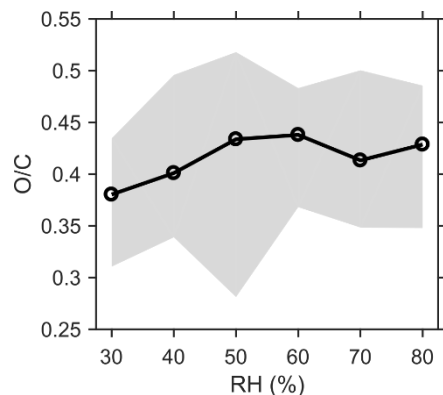


**Figure S13.** Submicron particle organic aerosol atomic O/C ratios as a function of RH. Data are measured by the AMS and grouped in RH bins (10% increment). The shaded region indicates the 25<sup>th</sup> and 75<sup>th</sup> percentiles.

## Reference

- Bahreini, R., Ervens, B., Middlebrook, A. M., Warneke, C., de Gouw, J. A., DeCarlo, P. F., Jimenez, J. L., Brock, C. A., Neuman, J. A., Ryerson, T. B., Stark, H., Atlas, E., Brioude, J., Fried, A., Holloway, J. S., Peischl, J., Richter, D., Walega, J., Weibring, P., Wollny, A. G., and Fehsenfeld, F. C.: Organic aerosol formation in urban and industrial plumes near Houston and Dallas, Texas, *J. Geophys. Res.-Atmos.*, 114, D00F16, doi:10.1029/2008JD011493, 2009.
- Du, Z., He, K., Cheng, Y., Duan, F., Ma, Y., Liu, J., Zhang, X., Zheng, M., and Weber, R.: A yearlong study of water-soluble organic carbon in Beijing I: Sources and its primary vs. secondary nature, *Atmos. Environ.*, 92, 514-521, doi:10.1016/j.atmosenv.2014.04.060, 2014.
- Fountoukis, C., and Nenes, A.: ISORROPIA II: a computationally efficient thermodynamic equilibrium model for  $\text{K}^+$ - $\text{Ca}^{2+}$ - $\text{Mg}^{2+}$ - $\text{NH}_4^+$ - $\text{Na}^+$ - $\text{SO}_4^{2-}$ - $\text{NO}_3^-$ - $\text{Cl}^-$ - $\text{H}_2\text{O}$  aerosols, *Atmos. Chem. Phys.*, 7, 4639-4659, doi:10.5194/acp-7-4639-2007, 2007.
- Guo, H., Weber, R. J., and Nenes, A.: High levels of ammonia do not raise fine particle pH sufficiently to yield nitrogen oxide-dominated sulfate production, *Sci. Rep.*, 7, 12109, doi:10.1038/s41598-017-11704-0, 2017.

Huang, K., Zhuang, G., Wang, Q., Fu, J. S., Lin, Y., Liu, T., Han, L., and Deng, C.: Extreme haze pollution in Beijing during January 2013: chemical characteristics, formation mechanism and role of fog processing, *Atmos. Chem. Phys. Discuss.*, 2014, 7517-7556, doi:10.5194/acpd-14-7517-2014, 2014.

Huang, X.-F., Hu, M., He, L.-Y., and Tang, X.-Y.: Chemical characterization of water-soluble organic acids in PM<sub>2.5</sub> in Beijing, China, *Atmos. Environ.*, 39, 2819-2827, doi:10.1016/j.atmosenv.2004.08.038, 2005.

Jiang, B., Kuang, B. Y., Liang, Y., Zhang, J., Huang, X. H. H., Xu, C., Yu, J. Z., and Shi, Q.: Molecular composition of urban organic aerosols on clear and hazy days in Beijing: a comparative study using FT-ICR MS, *Environ. Chem.*, 13, 888-901, doi:10.1071/EN15230, 2016.

Liu, M., Song, Y., Zhou, T., Xu, Z., Yan, C., Zheng, M., Wu, Z., Hu, M., Wu, Y., and Zhu, T.: Fine particle pH during severe haze episodes in northern China, *Geophys. Res. Lett.*, 44, 5213-5221, doi:10.1002/2017GL073210, 2017.

Pye, H. O. T., Liao, H., Wu, S., Mickley, L. J., Jacob, D. J., Henze, D. K., and Seinfeld, J. H.: Effect of changes in climate and emissions on future sulfate-nitrate-ammonium aerosol levels in the United States, *J. Geophys. Res.-Atmos.*, 114, D01205, doi:10.1029/2008JD010701, 2009.

Seinfeld, J. H., and Pandis, S. N.: *Atmospheric chemistry and physics: from air pollution to climate change*, Third ed., John Wiley & Sons, Inc., Hoboken, New Jersey, 2016.

Wang, G., Zhang, R., Gomez, M. E., Yang, L., Levy Zamora, M., Hu, M., Lin, Y., Peng, J., Guo, S., Meng, J., Li, J., Cheng, C., Hu, T., Ren, Y., Wang, Y., Gao, J., Cao, J., An, Z., Zhou, W., Li, G., Wang, J., Tian, P., Marrero-Ortiz, W., Secrest, J., Du, Z., Zheng, J., Shang, D., Zeng, L., Shao, M., Wang, W., Huang, Y., Wang, Y., Zhu, Y., Li, Y., Hu, J., Pan, B., Cai, L., Cheng, Y., Ji, Y., Zhang, F., Rosenfeld, D., Liss, P. S., Duce, R. A., Kolb, C. E., and Molina, M. J.: Persistent sulfate formation from London Fog to Chinese haze, *Proc. Natl. Acad. Sci. U.S.A.*, 113, 13630-13635, doi:10.1073/pnas.1616540113, 2016.

Wang, J., Wang, G., Gao, J., Wang, H., Ren, Y., Li, J., Zhou, B., Wu, C., Zhang, L., Wang, S., and Chai, F.: Concentrations and stable carbon isotope compositions of oxalic acid and related SOA in Beijing before, during, and after the 2014 APEC, *Atmos. Chem. Phys.*, 17, 981-992, doi:10.5194/acp-17-981-2017, 2017.

Wang, Y., Zhuang, G., Chen, S., An, Z., and Zheng, A.: Characteristics and sources of formic, acetic and oxalic acids in PM<sub>2.5</sub> and PM<sub>10</sub> aerosols in Beijing, China, *Atmos. Res.*, 84, 169-181, doi:10.1016/j.atmosres.2006.07.001, 2007.

Yang, Y., Zhou, R., Wu, J., Yu, Y., Ma, Z., Zhang, L., and Di, Y.: Seasonal variations and size distributions of water-soluble ions in atmospheric aerosols in Beijing, 2012, *J. Environ. Sci.*, 34, 197-205, doi:10.1016/j.jes.2015.01.025, 2015.